PERIODICUM BIOLOGORUM
VOL. 127, No 3–4, 163–175, 2025
DOI: 10.18054/pb.v127i3-4.36855

UDC 57:61
CODEN PDBIAD
ISSN 0031-5362

Original research article

Structural and functional analysis of a novel flavonoid-binding hypothetical protein from *Staphylococcus aureus* through molecular docking and dynamics

UGUR COMLEKCIOGLU[1,*]
MUSTAFA SEVINDIK[2]
NAZAN COMLEKCIOGLU[1]

[1] Kahramanmaras Sutcu Imam University, Faculty of Science, Biology Department, Kahramanmaras, Turkey

[2] Osmaniye Korkut Ata University, Engineering and Natural Sciences Faculty, Biology Department, Osmaniye, Turkey

***Correspondence:**
Ugur Comlekcioglu
E-mail address: cugur@ksu.edu.tr

Keywords: *Staphylococcus aureus*; hypothetical proteins; polyphenols; hesperidin; docking

Abstract

Staphylococcus aureus *is a significant human pathogen responsible for a wide range of infections, with increasing antibiotic resistance posing a major global health challenge. Despite extensive genomic characterization, many hypothetical proteins remain functionally unannotated, limiting our understanding of bacterial adaptation and pathogenicity. This study aimed to characterize such hypothetical protein, YP_500302.1, to uncover their potential roles and therapeutic relevance. YP_500302.1 was identified as a 495-amino acid transmembrane protein, predicted to function as a glucosyltransferase. Structural and physicochemical analyses indicated its potential involvement in membrane-associated processes. Molecular docking studies with 35 polyphenols revealed that hesperidin (-9.5 kcal mol^{-1}), naringin (-9.3 kcal mol^{-1}), and rutin (-8.9 kcal mol^{-1}) exhibited the strongest binding affinities. Hydrogen bond analysis over a 10 ns molecular dynamics simulation further supported the dynamic interactions of hesperidin with key residues, particularly ASP32 and THR370. These findings highlight the importance of characterizing hypothetical proteins in* S. aureus *to identify novel drug targets and combat antibiotic resistance.*

INTRODUCTION

Staphylococcus aureus is a Gram-positive bacterium that serves as both a commensal organism and a potent pathogen. It is commonly found colonizing human skin and mucous membranes, with the nasal cavity being a primary reservoir *(1)*. *S. aureus* is a leading global contributor to morbidity and mortality from infectious agents. It can cause a wide range of illnesses, from relatively mild skin infections to serious conditions such as pneumonia and sepsis, which can be fatal *(2)*. The clinical management of *S. aureus* infections has become increasingly challenging due to its rapid evolution of antibiotic resistance. The emergence of methicillin-resistant *S. aureus* (MRSA), conferred by the mecA gene carried on the Staphylococcal Cassette Chromosome mec (SCCmec), is particularly concerning. MRSA strains have now spread beyond hospital settings to become prevalent in community environments as well *(3, 4)*. The situation is further exacerbated by the emergence of multidrug-resistant and vancomycin-resistant *S. aureus* (VRSA) strains, which represent a significant global health threat *(5)*. Whole-genome sequencing (WGS) is increasingly being used in clinical microbiology to predict

Received June 9, 2025
Revised October 2, 2025
Accepted October 3, 2025

antimicrobial resistance profiles and guide therapy. This approach offers high accuracy for predicting phenotypes compared to traditional methods *(6)*.

The latest advances in the genomics of *S. aureus* highlight its genetic complexity, adaptability, and the implications for disease management and antimicrobial resistance. Genomic studies have shown that *S. aureus* evolves through horizontal gene transfer, recombination events, and the acquisition of resistance genes on mobile genetic elements like the SCCmec. These genetic adaptations enable it to evade antibiotics and enhance its fitness in various environments *(7)*. Genomic studies of epidemic strains reveal large-scale genetic rearrangements and acquisitions of resistance and virulence genes. These findings have significant implications for tracking outbreaks and understanding the mechanisms driving pathogenicity *(8)*.

The genomic intricacy of *S. aureus* underscores the breadth of its adaptive strategies, including resistance acquisition and virulence enhancement. However, despite extensive genomic characterization, a substantial portion of the *S. aureus* proteome remains poorly understood, with many encoded proteins classified as hypothetical. These hypothetical proteins are predicted from genomic data but lack experimentally validated functions, representing an enigmatic aspect of the organism's biology *(9)*. Delving into the roles of these proteins could uncover novel mechanisms of pathogenicity, resistance, and survival, providing critical insights into the molecular underpinnings of *S. aureus* as both a commensal and a pathogen *(10, 11)*. These efforts are not only essential for filling gaps in genomic annotations but also for identifying potential targets for therapeutic intervention in the context of antibiotic resistance *(12)*. Because these proteins could be integral to processes that allow the bacterium to colonize hosts, evade immune responses, or adapt to hostile environments.

Predictive characterization studies on the reference strain *S. aureus* NCTC 8325 uncovered 35 hypothetical proteins. These were linked to processes such as iron transport, virulence, and cellular metabolism. Proteins such as superoxide dismutase and ABC transporters were identified as crucial for bacterial survival and virulence, underscoring their importance as potential therapeutic targets *(11)*. Another study by Mohan and Venugopal *(9)* explored the structural and functional aspects of ten hypothetical proteins using bioinformatics tools. Their work identified domains related to transport proteins, ribosomal proteins, and arsenate reductases, among others. These findings suggested that hypothetical proteins could be linked to antibiotic resistance and pathogenicity by participating in key metabolic or structural roles *(9)*. Methicillin-resistant *S. aureus* (MRSA) strains have been a focus of research due to their public health impact. Marklevitz and Harris *(12)* investigated hypothetical proteins expressed differentially in resistant strains, revealing that many had potential links to antibiotic resistance mechanisms. They emphasized the gap in functional annotation, noting that current methodologies must advance to characterize these proteins effectively *(12)*. YP_001317347.1, a hypothetical protein with a YbbR domain, was characterized as binding ribosomal subunits. Such findings are critical for understanding how *S. aureus* exploits its proteome for survival and adaptation *(13)*.

Hypothetical proteins constitute a significant portion of the *Staphylococcus aureus* proteome, representing sequences with uncharacterized functions. Characterizing these proteins is essential for understanding bacterial physiology, pathogenesis, and potential therapeutic targets. In this study, we performed a comparative genomic analysis of 16 *S. aureus* genomes to identify highly con-

Table 1. *Genomic characteristics of Staphylococcus aureus strains analyzed in this study.*

Strain	Genome size (Mb)	Completeness (%)	Contamination (%)	Accession
NCTC 8325*	2.8	97.59	0.59	NC_007795
CC239-MRSA-III	3.1	97.18	0.58	CP127024
DSM 20231	2.8	98.61	0.39	CP104478
HC1340	3.0	98.15	0.51	CP012011
LA MRSA ST398	2.8	98.90	0.39	CP013218
MRSA AMRF 5	2.9	98.25	0.34	CP062467
MRSA WC090	2.8	98.37	0.62	CP092563
MRSA11	2.9	98.17	0.39	CP127345
MRSA107	3.1	98.65	0.33	CP018629
MRSA252	2.9	97.44	0.68	NC_002952
NCCP14558	3.0	96.75	0.39	CP013953
NY2491	3.0	98.73	0.39	CP094855
RIVM M044329	2.9	98.9	1.22	CP096540
ST772 MRSA V	2.9	98.87	0.34	CP010526
TUM9463	3.1	98.02	0.58	AP019306
UTSW MRSA 55	3.0	97.99	1.60	CP013231

*Reference strain

served hypothetical proteins. Among the conserved hypothetical proteins, we prioritized transmembrane proteins because they often contribute to bacterial adaptation, virulence, and host interaction. Due to their surface localization and membrane-associated functions, they also represent accessible and attractive targets for drug and vaccine development. Hence, YP_500302.1 was selected for detailed investigation based on its predicted transmembrane and glycosyltransferase-like features. Molecular docking analyses revealed strong binding interactions with flavonoid glycosides, particularly hesperidin, naringin, and rutin. Molecular dynamics simulations further demonstrated stable ligand–protein interactions, suggesting YP_500302.1 as a promising candidate for functional annotation and as a potential therapeutic target. By elucidating these structural and functional traits, this study highlights how unexplored proteins in *S. aureus* may be leveraged to combat antibiotic resistance.

MATERIAL AND METHODS

Data mining

S. aureus genomes were retrieved from NCBI (National Center for Biotechnology Information) database (https://www.ncbi.nlm.nih.gov/). The completeness of the selected genomes was >90%, and the contamination levels of these genomes were less than 5% *(14)*. The genomes were retrieved from NCBI database in full GenBank (.gb) format for hypothetical protein analysis and fasta format (.fna) for average nucleotide identity analysis. The accession numbers and details of the respective genomes are provided in Table 1.

Extraction of hypothetical protein sequences

GenBank files corresponding to the genome sequences of *S. aureus* were processed to identify CDS and their associated product annotations. A Python-based script was developed to parse GenBank files and quantify CDS, product annotations, gene counts, hypothetical protein counts, and non-hypothetical gene counts. A second script was implemented to specifically extract amino acid sequences of hypothetical proteins from the GenBank files. A total of 8120 hypothetical proteins were obtained from 16 *S. aureus* genomes. Then, sequences annotated as "hypothetical protein" were categorized based on their lengths. To investigate the homology among hypothetical proteins, a pairwise comparison of protein sequences was conducted using Biopython's Pairwise Aligner module with the BLOSUM62 substitution matrix. Sequences were filtered based on a user-defined length range and analyzed for local sequence alignment. A similarity threshold of 95% and occurrence rate of 90% in 16 *S. aureus* genomes were employed to determine homologous relationships. After homologous analysis, 138 hypothetical proteins were subjected to PSORTb *(15)*, ProtCompB (www.softberry.com), and CELLO *(16)* servers to find protein's sub-cellular location. Finally, 14 membrane-associated hypothetical proteins were used for further analysis.

Determination of physiochemical properties

Analysis of isoelectric point (pI), instability index (II, stability of proteins), aliphatic index (AI, relative volume of protein occupied by aliphatic side chains) and Grand Average of Hydropathicities (GRAVY, sum of all hydropathicity values of all amino acids divided by number of residues in a sequence) were done by using ExPASy-ProtParam server *(17)*. The predicted protein solubility is calculated by using Protein-Sol server. The scaled solubility value (QuerySol) is the predicted solubility. The population average for the experimental dataset (PopAvrSol) is 0.45, and thus any scaled solubility value greater than 0.45 is predicted to have a higher solubility than the average soluble *E. coli* protein from the experimental solubility dataset. The protein with a lower scaled solubility value is predicted to be less soluble *(18)*.

Structure and functional analysis

Putative conserved domains were detected in CDD-BLAST. The InterPro server was also used to assign the functional categories of motifs which provide the most probable match through evaluating the maximum similarity score. The VirulentPred 2.0 *(19)* and VICMpred *(20)* tools were used to identify virulence factors among the hypothetical proteins. The allergenicity of the peptides was checked using the AllergenFP 1.0 *(21)* and AllerTOP 2.0 *(22)* servers.

Secondary structure of the selected candidate protein (YP_500302.1) was performed using SOPMA tool in prabi by calculating the number of α-helices, turn, extended strand, random coil. To utilize SOPMA, amino acid sequence of the protein has been submitted in FASTA format. The experimentally uncharacterized 3D structure of YP_500302.1 was obtained from the AlphaFold Protein Structure Database (AF-Q2FXN8-F1) for *S. aureus* NCTC 8325. The tertiary structure of the protein has been evaluated by using ProSA-Web *(23)*, ERRAT *(24)*, Verify 3D *(25)* and PROCHECK *(26)*.

Molecular docking and post-docking analysis

The protein structure was processed using AutoDockTools 1.5.7 to remove water molecules and add polar hydrogens. Kollman and Gasteiger charges were assigned to all atoms of the protein to ensure proper charge distribution. A set of 35 plant-derived polyphenols, including flavonoids, phenolic acids, proanthocyanidins, and stilbenes, were selected for docking analysis based on their reported antimicrobial properties. The ligand structures

were retrieved from the PubChem database in SDF format; energy minimization of the ligands was performed using MMFF94 force field.

To define the docking search space, CASTpFold (Computed Atlas of Surface Topography of proteins) was used to identify potential binding pockets *(27)*. Based on the largest predicted binding pocket, a grid box was set up with dimensions ensuring complete coverage of the active site. Docking simulations were carried out using AutoDock Vina with num_modes set to 20 to explore multiple binding poses for each ligand. The exhaustiveness parameter was set to 32 to balance computational efficiency and accuracy. The docking calculations generated binding poses ranked by binding free energy (ΔG, kcal/mol). The top binding modes for each ligand were analyzed based on binding energy and hydrogen bond interactions using UCSF ChimeraX *(28)*, Discovery Studio Visualizer, and LigPlot+ *(29)*. The best ligand pose was selected from the ligand-protein complex file, and interactions, including hydrogen bonds, were mapped *(30)*.

Molecular dynamics simulation (MD simulation) and trajectory analysis

Molecular dynamics (MD) simulations were conducted using the GROMACS 2021.4 software package *(31)*. Atomistic simulations were performed for a solvated protein system at the experimental temperature of 37°C. The CHARMM27 force field *(32)* and TIP3P water model *(33)* were employed. The simulation box was defined as a cubic box with a 1.0 nm distance between the protein and the box edges to ensure compliance with the minimum image convention. This configuration guaranteed that the short-range interaction force cut-off distance did not exceed half the box length, preventing atoms from interacting with their own periodic images.

The system's ionic composition was further adjusted to neutralize the net charge of the protein. All systems underwent energy minimization using the steepest descent algorithm to remove unfavorable contacts, ensuring a stable starting configuration for equilibration. Equilibration was carried out in two steps. First, a constant volume and temperature (NVT) ensemble was simulated using a velocity-rescaling thermostat to maintain the system temperature at 310 K (37°C). This was followed by a constant pressure and temperature (NPT) ensemble, where the Parrinello–Rahman barostat *(34)* was employed to stabilize the pressure at 1 bar. During equilibration, positional restraints of 1000 kJ/mol/nm² were applied to the protein backbone to allow the solvent and ions to relax around the protein.

Production simulations were performed with a time step of 2 fs using the leap-frog integrator. Production simulations were carried out for a total of 10 ns for each experimental condition. After the simulations, GROMACS was utilized to evaluate both global and local structural changes in protein. These analyses included assessing the root-mean-squared deviation (RMSD) of the backbone atoms for structural stability, the root-mean-squared fluctuation (RMSF) of individual residues for flexibility, the solvent-accessible surface area (SASA) to measure solvent exposure, and the radius of gyration (Rg) to track changes in the protein's overall compactness *(35)*.

MM-PBSA Calculations

The binding free energies (ΔG_{bind}) of the protein-ligand complexes were calculated using the molecular mechanics Poisson–Boltzmann surface area (MM-PBSA) method, implemented in gmx_MMPBSA v1.6.4 *(36)*. The calculations were performed using the adaptive Poisson–Boltzmann solver (APBS 3.0) to evaluate solvation energy contributions. In the MM-PBSA framework, the binding free energy (ΔG_{bind}) of a protein-ligand complex in solution is defined as:

$$\Delta G_{\text{bind}} = G_{\text{complex}} - (G_{\text{protein}} + G_{\text{ligand}})$$

where $G_{complex}$ represents the total free energy of the protein-ligand complex, and $G_{protein}$ and G_{ligand} denote the free energies of the separated protein and ligand in solution, respectively. The energy decomposition analysis included van der Waals interactions, electrostatic interactions, polar solvation energy, and non-polar solvation energy. The calculations were based on molecular dynamics (MD) trajectories obtained from GROMACS (v2021.4) simulations. To ensure accuracy, periodic boundary conditions were removed, and structures were properly aligned before analysis.

RESULTS

Identification of hypothetical proteins

The counts of coding sequences (CDSs), hypothetical proteins, and non-hypothetical gene products were extracted and the distribution of hypothetical and non-hypothetical proteins across the analysed genomes is presented in Figure 1. This analysis was conducted using annotated genomic data of multiple *S. aureus* strains obtained from NCBI. Across the genomes, a significant proportion of CDSs were annotated as hypothetical proteins. The percentage of hypothetical proteins varied between genomes, indicating gaps in functional annotation and gene prediction pipelines. The dataset revealed intergenomic variability, with some genomes exhibiting a markedly higher number of hypothetical proteins. These differences may reflect strain-specific genomic adaptations or incomplete annotation databases.

The highest number of hypothetical proteins was found in strain NCTC8325 with a total number of 1496 proteins, nearly half of the genomic proteins (54.3%).

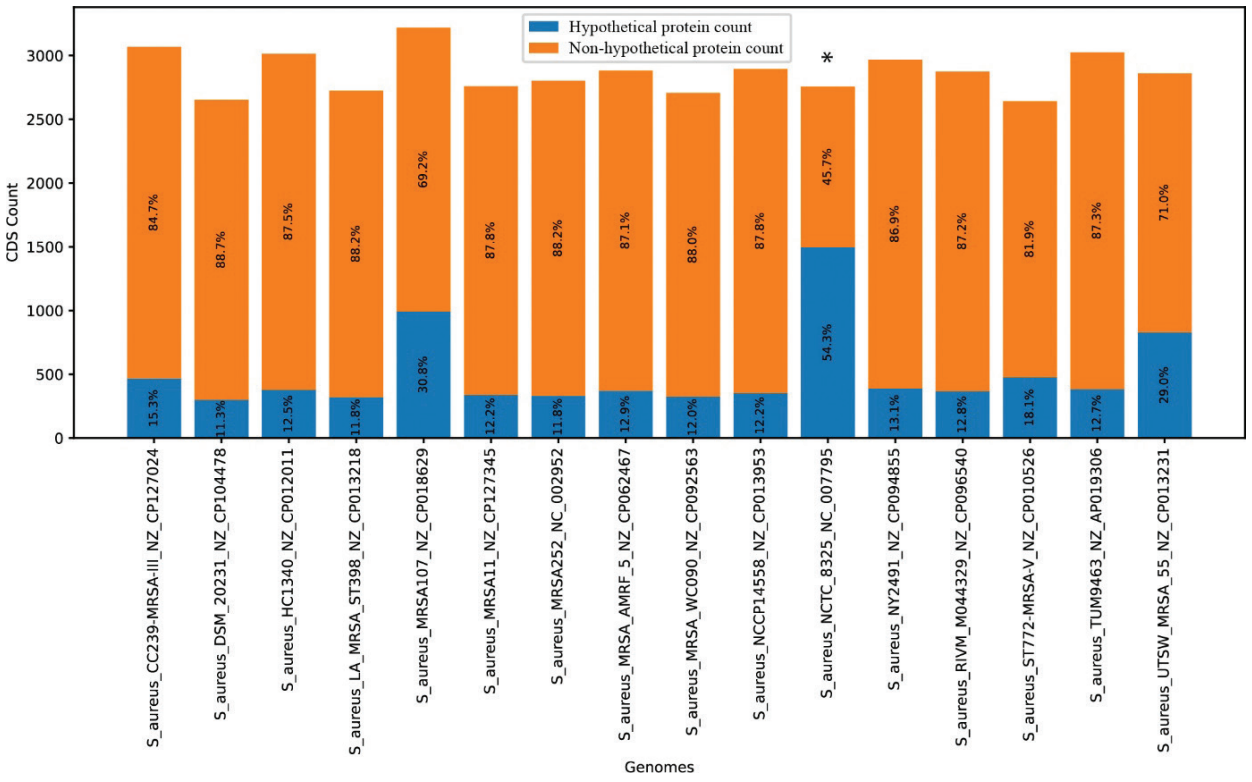

Figure 1. *Comparative analysis of hypothetical vs non-hypothetical protein coding sequences (CDS) across S. aureus genomes. This bar chart displays the count and percentage distribution of hypothetical and non-hypothetical protein-coding sequences (CDS) across various S. aureus genomes. *Indicates reference genome.*

High hypothetical protein rates were also found in strain MRSA107 (30.8%) and UTSW MRSA 55 (29%), however, the other genomes had much more annotated genes and the ratio of hypothetical proteins ranged between 11.3-18.1%. The amino acid sequence lengths of hypothetical proteins exhibited considerable variability across all genomes analyzed. These proteins ranged from as short as 29–100 amino acids to more than 2000 amino acids. The histogram in Figure 2A and 2B represents the combined frequency distribution of hypothetical protein lengths pooled from all analyzed *S. aureus* genomes. The majority of hypothetical proteins were shorter than 200 amino acids, and their overall frequency progressively decreased as sequence length increased.

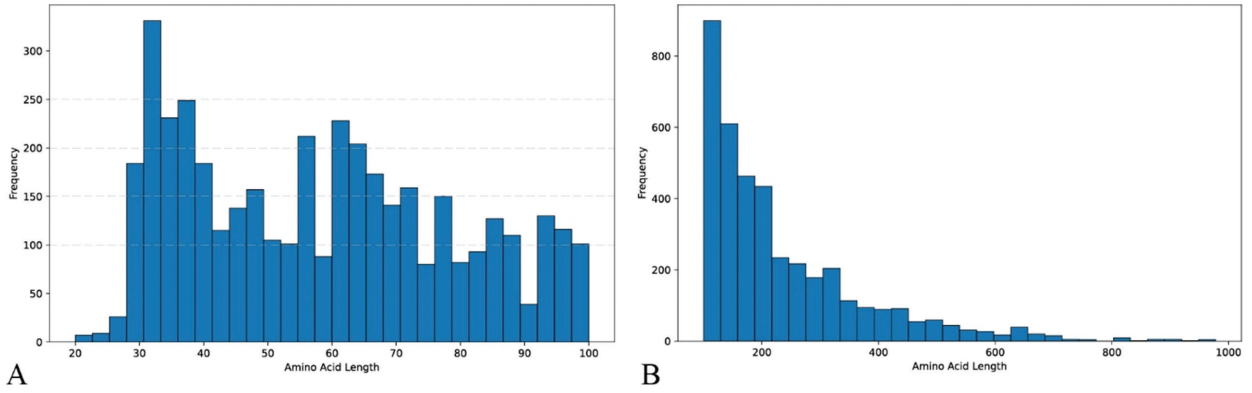

Figure 2. ***(A)*** *Distribution of hypothetical protein lengths ranging from 20 to 100 amino acids. The histogram illustrates the frequency of hypothetical proteins across different amino acid length intervals, with the highest frequency observed for proteins approximately 30-40 amino acids long, indicating a predominance of shorter hypothetical proteins within this dataset.* ***(B)*** *Distribution of hypothetical protein lengths ranging from 100 to 1000 amino acids. The histogram demonstrates a skewed distribution with the majority of proteins concentrated in the 100-200 amino acid range, gradually decreasing in frequency as protein length increases.*

Screening of transmembrane proteins among homologous hypothetical proteins

Hypothetical proteins ranging from 100 to 500 amino acids in length and present in at least 15 out of the 16 *S. aureus* genomes analyzed were examined for their transmembrane properties. PSORTb predicted 16 proteins, ProtCompB predicted 19 proteins and CELLO predicted 14 proteins as membrane-associated. The three servers predicted 14 hypothetical proteins as membrane proteins in common. Table 2 lists the proteins predicted as membrane proteins. InterProScan confirmed the presence of transmembrane regions in these proteins. A domain belonging to the 6TM ABC transporter family was detected in YP_499909.1 and a domain belonging to the DUF6056 superfamily was detected in YP_500302.1, but no conserved domains were detected in other proteins. VirulentPred predicted all proteins as virulent, on the other hand all proteins were predicted as probable nonallergen by both AllergenFP and AllerTOP servers. The proteins with the highest number of transmembrane helices (TMHs) detected by DeepTMHMM-1.0 were YP_499181.1 (6 TMHs), YP_499277.1 (7 TMHs) and YP_500302.1 (13 TMH). Among them, YP_500302.1 (gene symbol: SAOUHSC_01798) was selected for further analysis.

Structural and functional analysis of YP_500302.1

The SOPMA server was used to determine the secondary structure percentages of YP_500302.1, which include alpha helix (63.23%), random coil (28.89%), and extended strand (7.88%). The isoelectric point (pI) was determined as 9.42, indicating a basic nature. The Grand Average of Hydropathicity Index (GRAVY) value of 0.604 suggests that the protein is hydrophobic, indicating a potential preference for interaction with lipid environments such as membranes or hydrophobic regions of other molecules. The instability index (II) of 37.24 classifies the protein as stable under normal conditions, as values below 40 indicate protein stability. Additionally, the high aliphatic index of 124.65 reflects the abundance of aliphatic side chains (alanine, valine, isoleucine, and leucine), suggesting that the protein may maintain structural stability over a wide range of temperatures. A STRING network enrichment analysis revealed that YP_500302.1 is associated with several functional clusters, indicating its involvement in diverse biological processes (Figure 3). The most enriched cluster, "YSIRK type signal peptide and Glycosyl transferase family 2", suggests a role in extracellular matrix organization and cell wall remodeling, with potential secretion or membrane association due to the YSIRK signal peptide and carbohydrate modification linked to glycosyl transferase activity. Another cluster, "Prophage tail endopeptidase and Phage tail tape measure protein", indicates a potential association with bacteriophage-related processes, implying a role in stress responses or phage component interactions. Homology to humans was predicted using BLASTp against the human proteome (taxid: 9606) available in the NCBI database and no significant similarity found.

The 3D structure of YP_500302.1 (SAOUHSC_01798) was obtained from the AlphaFold Protein Structure Database as the model AF-Q2FXN8-F1 for *S. aureus* NCTC 8325 (Figure 4). The quality of this AlphaFold model was assessed using multiple validation metrics. The QMEAN-DisCo global score was 0.59, and the QMEAN4 score was -3.06, indicating a moderately reliable model. The ProSA Z-score of -5.1 aligns well with scores for experimentally solved structures of similar size, supporting the overall structural accuracy of the model. VoroMQA yielded a score of 0.527, suggesting moderate local structure quality.

Table 2. *Conserved domain analysis, virulence predictions, and transmembrane helix predictions of hypothetical proteins from S. aureus.*

Protein	Sequence length	Conserved domain	VicmPred	VirulentPred	TMH
YP_501254	102	-	Metabolism	Virulent	3
YP_499407.1	104	-	Metabolism	Virulent	4
YP_499909.1	114	6TM ABC transporter family	Metabolism	Virulent	3
YP_501053	118	-	Cellular process	Virulent	4
YP_500980.1	129	-	Cellular process	Virulent	4
YP_500481	131	-	Metabolism	Virulent	4
YP_501378.1	138	-	Metabolism	Virulent	4
YP_500400.1	147	-	Metabolism	Virulent	2
YP_499356.1	152	-	Cellular process	Virulent	4
YP_498655.1	160	-	Metabolism	Virulent	4
YP_499277.1	194	-	Cellular process	Virulent	7
YP_501089.1	212	-	Metabolism	Virulent	4
YP_499181.1	238	-	Cellular process	Virulent	6
YP_500302.1	495	DUF6056 super family	Metabolism	Virulent	13

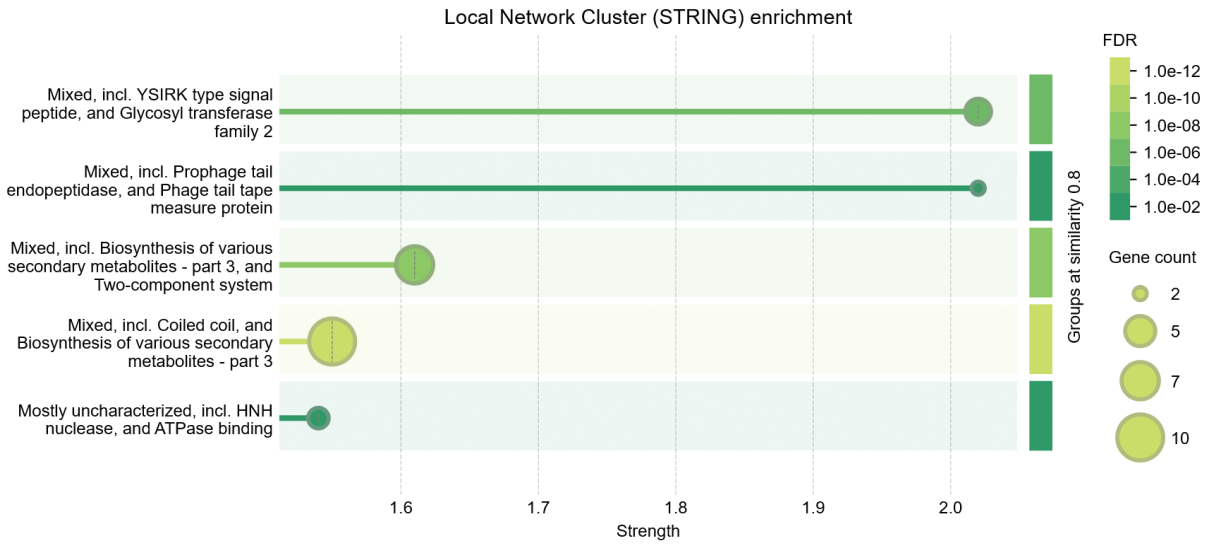

Figure 3. *STRING network enrichment analysis for YP_500302.1 and its interacting proteins. The identified clusters are ranked based on their strength scores, with higher values indicating stronger enrichment. The color gradient represents the statistical significance of the clusters (FDR), with lighter colors indicating higher significance, and the circle size denotes the number of genes involved in each cluster.*

The ERRAT value of 98.55% demonstrates good structural reliability. Verify3D analysis showed that 34.95% of the residues had an average 3D-1D score ≥ 0.2, indicating reasonable compatibility between the sequence and structure. Furthermore, the Ramachandran plot analysis revealed that 93.7% of residues were in allowed regions, with no residues in disallowed regions, underscoring the high stereochemical quality of the model. Collectively, based on these physicochemical and structural properties, the AlphaFold model for YP_500302.1 (AF-Q2FXN8-F1) was accepted as being of sufficient quality for further computational and functional analyses. The CASTpFold analysis of YP_500302.1 identified two prominent surface pockets. The largest pocket exhibited a surface area of 773.615 Å² and a volume of 745.448 Å³, while the second largest pocket had a surface area of 129.638 Å² and a volume of 233.026 Å³.

These findings highlight potential binding sites that may play critical roles in the protein's interaction with ligands or other biomolecules, making these pockets ideal targets for docking studies to elucidate the functional and structural relevance of YP_500302.1. A total of 35 polyphenols, including flavonoids, phenolic acids, proanthocyanidins, and stilbenes, were analyzed for their binding affinities to YP_500302.1 using Autodock Vina (Figure 5). The binding energies ranged from –5.4 kcal mol^{-1} to –9.5 kcal mol^{-1}, reflecting varying interaction strengths be-

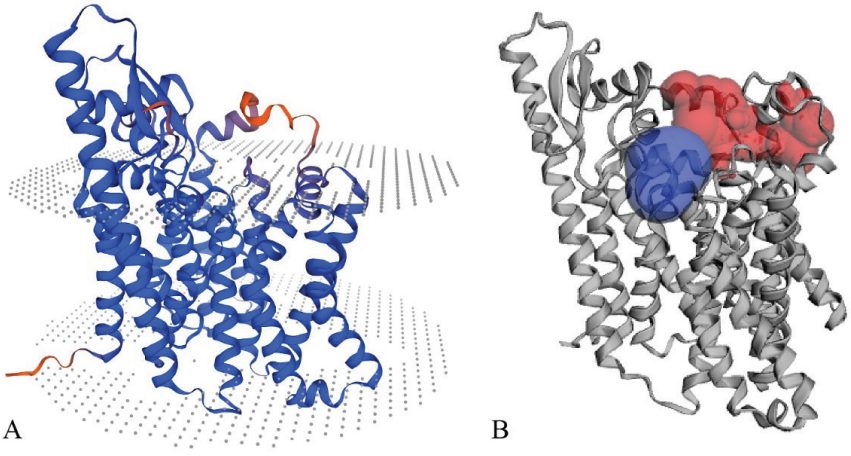

Figure 4. *Structural representation of YP_500302.1. (**A**) The 3D structure of AF-Q2FXN8-F1 (**B**) Surface pockets identified by CASTpFold, where the largest pocket is highlighted in red and the second largest pocket in blue.*

tween the protein and the polyphenols. The highest binding energies, corresponding to weaker interactions, were predominantly observed among phenolic acids (e.g., salicylic acid, gallic acid, and caffeic acid), ranging from -5.4 to -6.8 kcal mol^{-1}. In contrast, flavonoid glycosides such as hesperidin (-9.5 kcal mol^{-1}, K_i=0.178 µM), naringin (-9.3 kcal mol^{-1}, K_i=0.091 µM), and rutin (-8.9 kcal mol^{-1}, K^i=0.251 µM) exhibited the lowest binding energies, indicating the strongest binding affinities. These results suggest that flavonoid glycosides are the most promising candidates for targeting YP_500302.1 due to their high binding efficiency and structural similarity to substrates commonly associated with glycosyltransferases. According to UniProt, YP_500302.1 is a hypothetical uncharacterized transmembrane protein predicted to function as a glucosyltransferase. However, this annotation is based on bioinformatic predictions and remains experimentally unverified. UDP_GlcNAc and UDP_Glucose, which are commonly recognized substrates of glycosyltransferases, showed binding energies of -7.5 and -7.6 kcal mol^{-1}, respectively. The lower binding energies of flavonoid glycosides compared to these potential substrates highlight their competitive binding potential to the protein's active site. Further experimental studies are required to verify whether YP_500302.1 possesses glucosyltransferase activity and to confirm its substrate specificity.

Among the flavonoids, hesperidin formed four conventional hydrogen bond interactions with the protein residues ASP32, TYR469, LEU52, and GLN35 (Figure 6). Similarly, naringin and rutin exhibited six (ASP32, GLN35, GLU62, TRP36, TYR230, ARG55) and seven (GLU373, GLN231, ARG55, GLU62, ASN127, ASN53, ASN59) hydrogen bond interactions, respectively. These interactions are key contributors to the high binding affinity of these molecules. Furthermore, the flavonoid aglycones (e.g., quercetin, luteolin, and apigenin) demonstrated moderate binding energies (–7.8 to –8.5 kcal mol^{-1}), underscoring the role of sugar groups in enhancing binding affinity. Hydrogen bond analysis over a 10 ns molecular dynamics simulation revealed key interactions between YP_500302.1 and hesperidin (Figure 7). The residue ASP32 formed stable hydrogen bonds consistently during the first 6 ns, suggesting its critical role in anchoring the ligand within the binding pocket. A transient interaction with TYR469 was observed from 0 to 4 ns, highlighting its role in initial docking stabilization. Notably, THR370 formed hydrogen bonds in the later stages (8–10 ns), indicating a shift in the ligand's orientation or the presence of a secondary binding site. Short-lived interactions with ASN219 at 2 and 3 ns further supported its auxiliary role during the early binding phase. These findings underscore the dynamic nature of the binding process, with ASP32 playing a dominant role

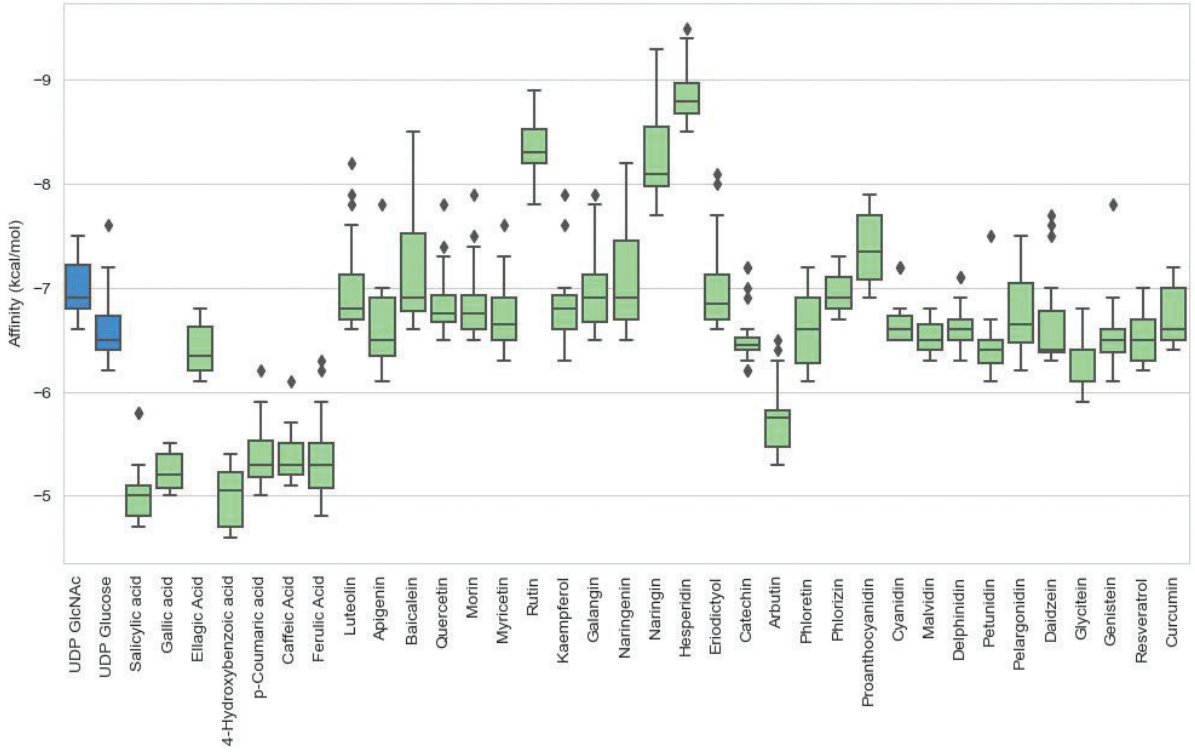

Figure 5. *Binding energy distributions of 35 polyphenols and two UDP derivatives (UDP-GlcNAc and UDP-Glucose) with YP_500302.1, as determined by molecular docking analysis. UDP derivatives, shown in blue, represent potential substrates for glycosyltransferases, while the polyphenols, shown in green, exhibit a wide range of binding affinities. Boxplots were generated based on the top 20 binding poses from docking simulations, with outliers representing variations in docking poses.*

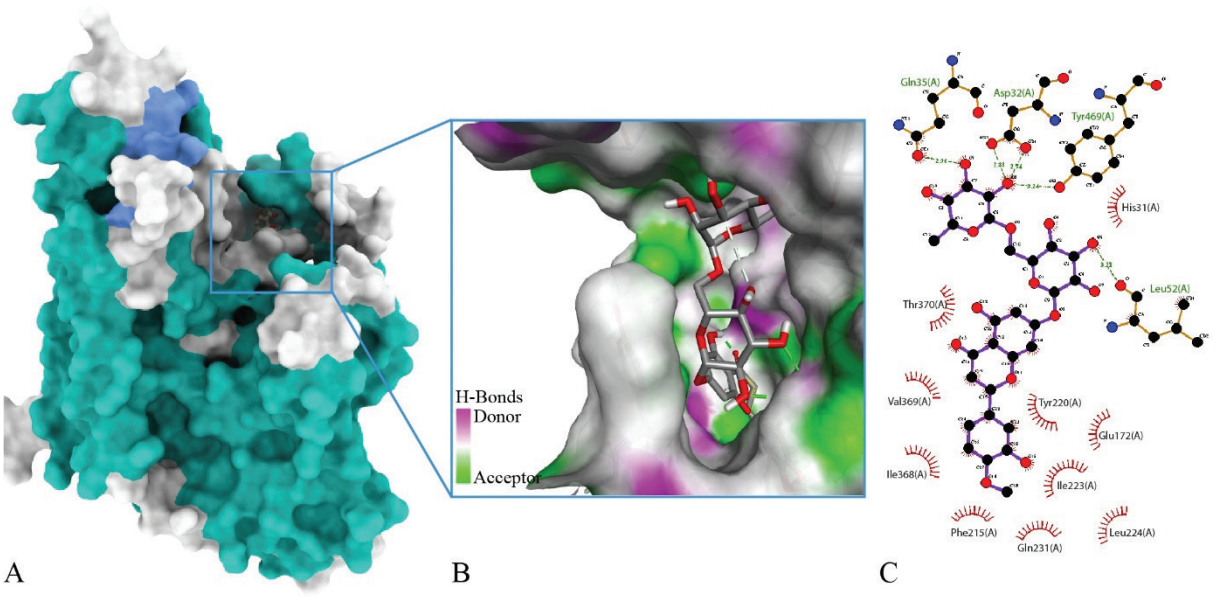

Figure 6. *Molecular docking and interaction analysis of hesperidin with YP_500302.1. (**A**) The surface representation of YP_500302.1 showing the binding pocket of hesperidin. (**B**) Detailed view of the docking pose within the binding cavity, highlighting the ligand orientation. Interaction map illustrates hydrogen bond donors (purple) and acceptors (green) within the binding site. (**C**) Two-dimensional representation of hesperidin's interactions with key amino acid residues in the active site at 0 ns, showing hydrogen bonds (green dashed lines), along with hydrophobic interactions. Distances are provided in angstroms.*

in initial stabilization and THR370 contributing to adaptive binding in the later stages.

The binding free energy of the YP_500302.1–hesperidin complex was evaluated using the Molecular Mechanics Poisson-Boltzmann Surface Area (MMPBSA) method, revealing favorable binding energetics (Figure 8). The van der Waals interactions contributed significantly to the binding energy with a ΔVDWAALS of -35.32 kcal/mol,

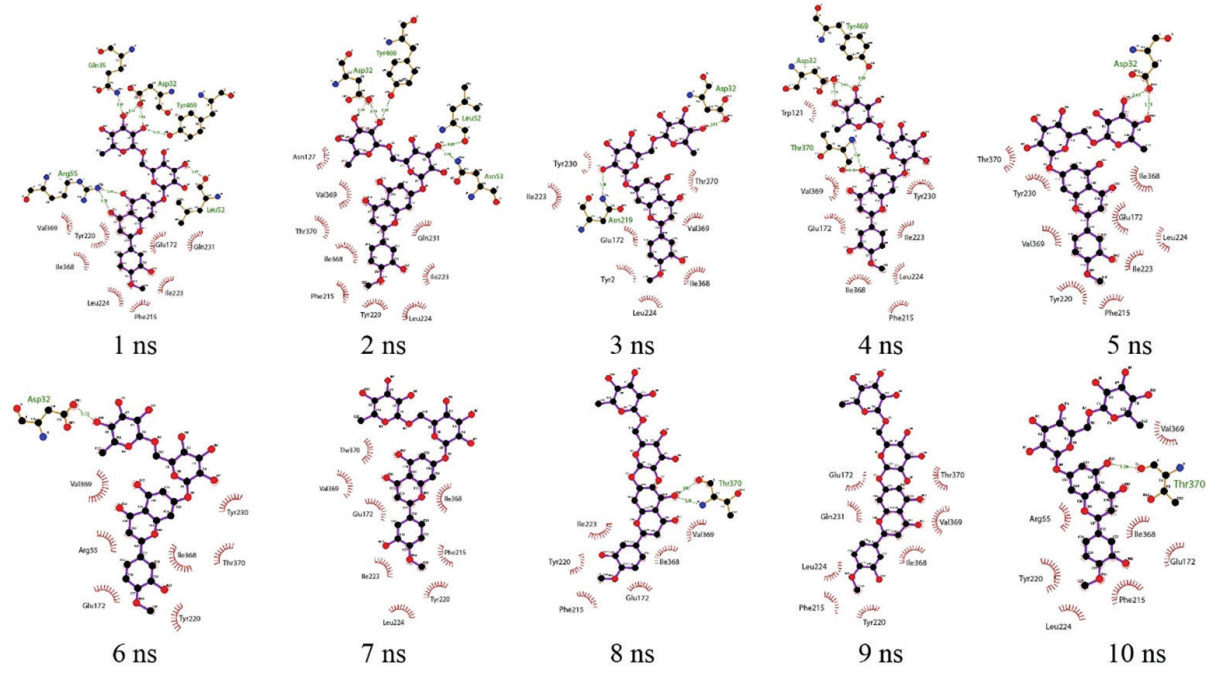

Figure 7. *Time-resolved hydrogen bond interactions of the hesperidin with YP_500302.1 over a 10 ns molecular dynamics simulation. Each snapshot represents the ligand's hydrogen bond interactions (green dashed lines) with key residues at specific time points (1–10 ns), highlighting changes in binding behavior and the dynamic nature of the protein-ligand complex. Distances are provided in angstroms.*

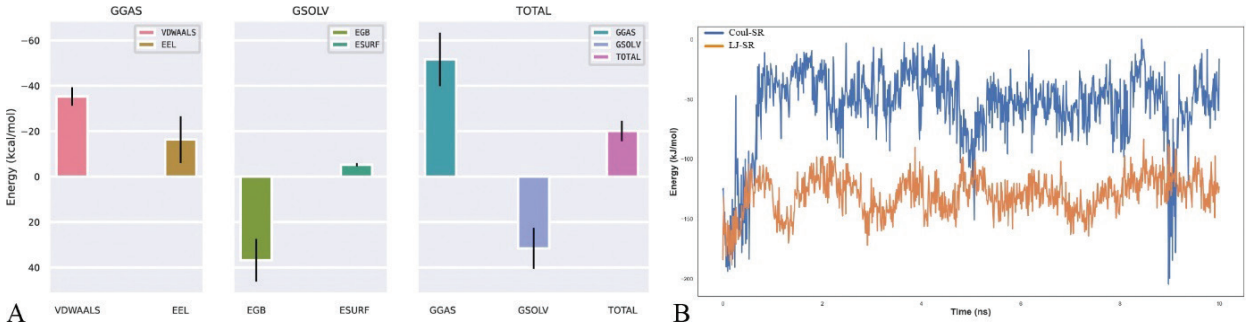

Figure 8. ***(A)*** *Energetic components of the hesperidin-YP_500302.1 complex calculated using the MM-PBSA approach. The bar graphs display contributions from gas-phase interactions (GGAS: van der Waals [VDWAALS] and electrostatic [EEL] energies), solvation energies (GSOLV: polar solvation [EGB] and non-polar solvation [ESURF]), and the total binding energy (ΔTOTAL). Error bars indicate standard deviations across the simulation frames.* ***(B)*** *Interaction energy analysis of the YP_500302.1–hesperidin complex during a 10 ns molecular dynamics simulation. The Lennard-Jones short-range (LJ-SR, orange line) energy represents van der Waals interactions, while the Coulombic short-range (Coul-SR, blue line) energy reflects electrostatic interactions.*

highlighting the importance of hydrophobic and non-covalent interactions in stabilizing the complex. This observation is further supported by the Lennard-Jones energy (LJ-SR) from molecular dynamics simulations, which exhibited an average value of -129.99 kJ/mol, indicating the dominance of van der Waals forces. Electrostatic interactions reinforced the binding, as indicated by an electrostatic energy (ΔEEL) of -16.33 kcal/mol, reflecting polar interactions such as hydrogen bonds with key residues (e.g., ASP32, TYR469, GLN35). This is consistent with the Coulombic short-range energy (Coul-SR), which averaged -56.10 kJ/mol, emphasizing the role of polar interactions in stabilizing the complex. Solvation energy analysis revealed contrasting contributions: while polar solvation energy (ΔEGB = +36.78 kcal/mol) introduced a penalty due to desolvation, this was partially offset by the favorable non-polar solvation energy (ΔESURF = -5.24 kcal/mol), driven by hydrophobic effects. The net binding free energy (ΔTOTAL= -20.10 kcal/mol) demonstrated a favorable interaction between hesperidin and YP_500302.1, driven primarily by van der Waals and electrostatic forces. These findings are consistent with the binding affinity observed in docking and molecular dynamics simulations, further validated by the stability of interaction energies during the 10 ns simulation.

DISCUSSION

Identifying alternative therapeutic targets is essential to combat pathogenic *S. aureus*. Several approaches are utilized to investigate potential drug targets, such as species-specific genes, uncharacterized genes, unique enzymes, virulence-associated factors, and membrane transporters *(37)*. Hypothetical proteins have gained attention as potential sources for alternative therapeutic targets due to their unknown functions and widespread presence in bacterial genomes *(38, 39)*. In this context, hypothetical proteins with unknown functions represent promising candidates, particularly those associated with membrane processes and bacterial adaptation mechanisms. In this study, we focused on such proteins, YP_500302.1, which were selected based on their predicted role and structural properties. The structural prediction and validation of this protein provide valuable insights into their potential functions and importance in the biology of *S. aureus*.

School et al. *(11)* analyzed 35 hypothetical proteins in *S. aureus* and found that these proteins are associated with virulence, protein-protein interactions, metabolism, and transport processes, highlighting their potential functional significance. YP_500302.1 was identified as a 495-amino acid hypothetical transmembrane protein with 13 predicted transmembrane helices, classified as a potential glucosyltransferase according to UniProt annotations. Structural and physicochemical analyses revealed its predominantly α-helical nature, basic isoelectric point (pI 9.42), and hydrophobic character (GRAVY: 0.604), suggesting its association with membrane-related functions. To better understand its structural characteristics, 3D model were obtained from the AlphaFold database. AlphaFold has been recognized for its ability to predict high-quality protein structures with accuracy comparable to medium-resolution experimental models, particularly for small proteins *(40)*. This is consistent with our findings, where the AlphaFold model showed a ProSA *z*-score of -5.1 which is close to the *z*-scores of all experimentally determined protein chain database *(23)*. Furthermore, structural validation using the Ramachandran plot, a widely accepted tool for protein structure validation *(41)*, revealed no residues in disallowed regions for the AlphaFold model.

Despite its unknown function, genetic synteny analysis has revealed that YP_500302.1 homologs are conserved across various bacterial species, suggesting a role in stress response pathways, while its ability to compensate for disrupted teichoic acid biosynthesis in *S. aureus* indicates

its contribution to cell envelope integrity and adaptation *(42)*. Recent studies have shown that a subset of essential hypothetical proteins in *S. aureus* play key roles in enzymatic functions, transport mechanisms, and virulence, with some identified as potential drug targets *(10, 43)*. To improve our knowledge about YP_500302.1 of *S. aureus*, specifically regarding its structural and functional traits, and to investigate its potential as a target for plant phenolic compounds, we conducted molecular docking studies to evaluate its binding interactions with various polyphenols, including flavonoids, phenolic acids, proanthocyanidins, and stilbenes which have demonstrated antimicrobial activities *(44)*. Computational analysis revealed that flavonoid glycosides, particularly hesperidin, naringin, and rutin, exhibited the strongest binding affinities, suggesting their potential as competitive inhibitors of YP_500302.1. Notably, hydrogen bonding analysis over a 10 ns trajectory revealed dynamic interactions between hesperidin and key residues such as ASP32 and THR370, which stabilized the ligand within the binding pocket during early and late stages of the simulation, respectively. Hydrogen bonds with a distance greater than 5 Å were not considered significant interactions *(45)*. Therefore, the hydrogen bonds observed during the 10 ns trajectory were considered significant, as their distances remained below 5 Å. The MM-PBSA approach is widely used for estimating interaction energies in biomolecular complexes, providing insights into conformational fluctuations and energetic contributions that drive ligand binding *(46)*. The energetic components of the interaction between YP_500302.1 and hesperidin reveal that van der Waals interactions (VDWAALS) and electrostatic energy (EEL) were the primary contributors to the binding energy, while solvation energies (GSOLV) provided additional stabilization. These combined contributions culminated in a favorable total binding energy, highlighting the potential of hesperidin as a promising lead compound.

Consistent with the findings in this study, Verma et al. *(47)* demonstrated that hesperidin and naringin exhibit high binding affinities to *S. aureus* (MRSA) Penicillin Binding Protein-2a, with docking scores of –9.2 and –9.6 kcal/mol, respectively, and maintain stable interactions during 30 ns molecular dynamics simulations, further supporting the potential of natural flavonoids as effective adjuvant antimicrobial agents against resistant strains. Additionally, hesperidin treatment has been shown to significantly impede the production of lipase, hemolysin, autolysin, autoaggregation, and staphyloxanthin in *S. aureus (48)*. Similarly, rutin-loaded chitosan nanoparticles (Rut-CS NPs) exhibited significant antibacterial activity, reducing staphyloxanthin production by 43.31–89.63%, thereby increasing *S. aureus* susceptibility to hydrogen peroxide *(49)*. Furthermore, naringin-loaded PLGA nanospheres demonstrated strong antibacterial efficacy, killing 99.9% of *E. coli* and *S. aureus* at a concentration of 0.2 mg/mL within 24 hours *(50)*. The results of this study demonstrated the strong binding potential of hesperidin, naringin, and rutin to YP_500302.1, alongside their potent antimicrobial and antibiofilm properties against *S. aureus*, suggesting that this hypothetical protein could represent a promising target for further investigation in the pursuit of novel therapeutic strategies against *S. aureus*.

Molecular docking and dynamic simulations revealed strong binding affinities of flavonoid glycosides, particularly hesperidin, naringin, and rutin, to YP_500302.1, highlighting its potential as a target for natural agents. While these findings underscore the functional significance of YP_500302.1, experimental validation is required before considering YP_500302.1 as a potential therapeutic target against resistant *S. aureus* infections. A limitation of this study is that the MD simulations were performed in an aqueous environment without an explicit lipid bilayer and were limited to a relatively short timescale of 10 ns due to computational cost and resource constraints. As transmembrane proteins experience structural and electrostatic stabilization from surrounding lipids, future work should incorporate membrane-mimicking environments (e.g., POPC/POPE bilayers) to more accurately capture physiologically relevant dynamics and interactions. Additionally, extending the simulations to at least 50–100 ns will provide more comprehensive conformational sampling and yield more reliable binding energy estimates, particularly for MM/PBSA calculations and trajectory clustering.

Acknowledgements: *This research did not receive any specific grant from funding agencies in the public, commercial, or not-for-profit sectors.*

REFERENCES

1. TONG S, DAVIS J, EICHENBERGER E, HOLLAND T, FOWLER V 2015 Staphylococcus aureus infections: Epidemiology, pathophysiology, clinical manifestations, and management. Clin Microbiol Rev 28: 603-661. https://doi.org/10.1128/CMR.00134-14
2. CHEUNG GY, BAE JS, OTTO M 2021 Pathogenicity and virulence of Staphylococcus aureus. Virulence 12: 547-569. https://doi.org/10.1080/21505594.2021.1878688
3. GORDON RJ, LOWY FD 2008 Pathogenesis of methicillin-resistant Staphylococcus aureus infection. Clin Infect Dis 46 Suppl 5: S350-S359. https://doi.org/10.1086/533591
4. DELEO FR, CHAMBERS HF 2009 Reemergence of antibiotic-resistant Staphylococcus aureus in the genomics era. J Clin Invest 119: 2464-2474. https://doi.org/10.1172/JCI38226
5. PEACOCK SJ, PATERSON GK 2015 Mechanisms of methicillin resistance in Staphylococcus aureus. Annu Rev Biochem 84: 577-601. https://doi.org/10.1146/annurev-biochem-060614-034516
6. GORDON NC, PRICE JR, COLE K, EVERITT R, et al. 2014 Prediction of Staphylococcus aureus antimicrobial resistance by whole-genome sequencing. J Clin Microbiol 52: 1182-1191. https://doi.org/10.1128/JCM.03117-13

7. HOLDEN MTG, FEIL EJ, LINDSAY JA, PEACOCK SJ, et al. 2004 Complete genomes of two clinical Staphylococcus aureus strains: Evidence for the rapid evolution of virulence and drug resistance. Proc Natl Acad Sci U S A 101: 9786-9791. https://doi.org/10.1073/pnas.0402521101
8. GRAY RR, TATEM AJ, JOHNSON JA, ALEKSEYENKO AV, et al. 2011 Testing spatiotemporal hypothesis of bacterial evolution using methicillin-resistant Staphylococcus aureus ST239 genome-wide data within a Bayesian framework. Mol Biol Evol 28: 1593-1603. https://doi.org/10.1093/molbev/msq319
9. MOHAN R, VENUGOPAL S 2012 Computational structural and functional analysis of hypothetical proteins of Staphylococcus aureus. Bioinformation 8: 722-728. https://doi.org/10.6026/97320630008722
10. PRAVA J, PRANAVATHIYANI G, PAN A 2018 Functional assignment for essential hypothetical proteins of Staphylococcus aureus N315. Int J Biol Macromol 108: 765-774. https://doi.org/10.1016/j.ijbiomac.2017.10.169
11. SCHOOL K, MARKLEVITZ J, SCHRAM WK, HARRIS LK 2016 Predictive characterization of hypothetical proteins in Staphylococcus aureus NCTC 8325. Bioinformation 12: 209-214. https://doi.org/10.6026/97320630012209
12. MARKLEVITZ J, HARRIS LK 2017 Improved annotations of 23 differentially expressed hypothetical proteins in methicillin resistant S. aureus. Bioinformation 13: 104-110. https://doi.org/10.6026/97320630013104
13. BHARAT P, VARMA S, ADIMULAM Y, KODUKULA S 2015 In silico functional annotation of a hypothetical protein from Staphylococcus aureus. J Infect Public Health 8: 526-532. https://doi.org/10.1016/j.jiph.2015.03.007
14. BOWERS, R., KYRPIDES, N., STEPANAUSKAS, R. et al. 2017 Minimum information about a single amplified genome (MISAG) and a metagenome-assembled genome (MIMAG) of bacteria and archaea. Nat Biotechnol 35: 725-731. https://doi.org/10.1038/nbt.3893
15. YU NY, WAGNER JR, LAIRD MR, et al. 2010 PSORTb 3.0: Improved protein subcellular localization prediction with refined localization subcategories and predictive capabilities for all prokaryotes. Bioinformatics 26: 1608-1615. https://doi.org/10.1093/bioinformatics/btq249
16. YU CS, CHEN YC, LU CH, HWANG JK 2006 Prediction of protein subcellular localization. Proteins 64: 643-651. https://doi.org/10.1002/prot.21018
17. GASTEIGER E, HOOGLAND C, GATTIKER A, DUVAUD S, et al. 2005 Protein identification and analysis tools on the ExPASy server. In: Walker JM (ed) The Proteomics Protocols Handbook. Humana Press, pp 571-607. https://doi.org/10.1385/1-59259-890-0:571
18. HEBDITCH M, CARBALLO-AMADOR MA, CHARONIS S, CURTIS R, WARWICKER J 2017 Protein-Sol: A web tool for predicting protein solubility from sequence. Bioinformatics 33: 3098-3100. https://doi.org/10.1093/bioinformatics/btx345
19. GARG A, GUPTA D 2008 VirulentPred: A SVM based prediction method for virulent proteins in bacterial pathogens. BMC Bioinformatics 9: 62. https://doi.org/10.1186/1471-2105-9-62
20. SAHA S, RAGHAVA GPS 2006 VICMpred: SVM-based method for the prediction of functional proteins of gram-negative bacteria using amino acid patterns and composition. Genomics Proteomics Bioinformatics 4: 42-47. https://doi.org/10.1016/S1672-0229(06)60015-6
21. DIMITROV I, NANEVA L, DOYTCHINOVA I, BANGOV I 2014 AllergenFP: Allergenicity prediction by descriptor fingerprints. Bioinformatics 30: 846-851. https://doi.org/10.1093/bioinformatics/btt619
22. DIMITROV I, BANGOV I, FLOWER DR, DOYTCHINOVA I 2014 AllerTOP v.2-A server for in silico prediction of allergens. J Mol Model 20: 2278. https://doi.org/10.1007/s00894-014-2278-5
23. WIEDERSTEIN M, SIPPL MJ 2007 ProSA-web: Interactive web service for the recognition of errors in three-dimensional structures of proteins. Nucleic Acids Res 35: W407-W410. https://doi.org/10.1093/nar/gkm290
24. COLOVOS C, YEATES TO 1993 Verification of protein structures: Patterns of nonbonded atomic interactions. Protein Sci 2: 1511-1519. https://doi.org/10.1002/pro.5560020916
25. LÜTHY R, BOWIE JU, EISENBERG D 1992 Assessment of protein models with three-dimensional profiles. Nature 356: 83-85. https://doi.org/10.1038/356083a0
26. LASKOWSKI RA, MACARTHUR MW, MOSS DS, THORNTON JM 1993 PROCHECK: A program to check the stereochemical quality of protein structures. J Appl Crystallogr 26: 283-291. https://doi.org/10.1107/S0021889892009944
27. YE B, TIAN W, WANG B, LIANG J 2024 CASTpFold: Computed Atlas of Surface Topography of the universe of protein Folds. Nucleic Acids Res 52: W194-W199. https://doi.org/10.1093/nar/gkae415
28. MENG EC, GODDARD TD, PETTERSEN EF, et al. 2023 UCSF ChimeraX: Tools for structure building and analysis. Protein Sci 32: e4792. https://doi.org/10.1002/pro.4792
29. LASKOWSKI RA, SWINDELLS MB 2011 LigPlot+: Multiple ligand-protein interaction diagrams for drug discovery. J Chem Inf Model 51: 2778-2786. https://doi.org/10.1021/ci200227u
30. REHMAN MFU, AKHTER S, BATOOL AI, et al. 2021 Effectiveness of natural antioxidants against SARS-CoV-2: Insights from the in-silico world. Antibiotics 10: 1011. https://doi.org/10.3390/antibiotics10081011
31. ABRAHAM MJ, MURTOLA T, SCHULZ R, et al. 2015 GROMACS: High performance molecular simulations through multi-level parallelism from laptops to supercomputers. SoftwareX 1: 19-25. https://doi.org/10.1016/j.softx.2015.06.001
32. BROOKS BR, BROOKS CL III, MACKERELL AD JR, et al. 2009 CHARMM: The biomolecular simulation program. J Comput Chem 30: 1545-1614. https://doi.org/10.1002/jcc.21287
33. JORGENSEN WL, CHANDRASEKHAR J, MADURA JD, et al. 1983 Comparison of simple potential functions for simulating liquid water. J Chem Phys 79: 926-935. https://doi.org/10.1063/1.445869
34. PARRINELLO M, RAHMAN A 1981 Polymorphic transitions in single crystals: A new molecular dynamics method. J Appl Phys 52: 7182-7190. https://doi.org/10.1063/1.328693
35. LI G, JIA L, WANG K, SUN T, HUANG J 2023 Prediction of thermostability of enzymes based on the amino acid index (AAindex) database and machine learning. Molecules 28: 8097. https://doi.org/10.3390/molecules28248097
36. VALDÉS-TRESANCO MS, VALDÉS-TRESANCO ME, VALIENTE PA, MORENO E 2021 gmx_MMPBSA: A new tool to perform end-state free energy calculations with GROMACS. J Chem Theory Comput 17: 6281-6291. https://doi.org/10.1021/acs.jctc.1c00645
37. HASAN MA, KHAN MA, SHARMIN T, MAZUMDER MHH, CHOWDHURY AS 2016 Identification of putative drug targets in Vancomycin-resistant Staphylococcus aureus using computer aided protein data analysis. Gene 575: 132-143. https://doi.org/10.1016/j.gene.2015.08.044
38. ASSIS LM, NEDELJKOVIĆ M, DESSEN A 2017 New strategies for targeting and treatment of multi-drug resistant Staphylococcus aureus. Drug Resist Updat 31: 1-14. https://doi.org/10.1016/j.drup.2017.03.001

39. RÖHRIG C, HUEMER M, LORGÉ D, et al. 2020 Targeting hidden pathogens: Cell-penetrating enzybiotics eradicate intracellular drug-resistant Staphylococcus aureus. mBio 11: e00209-20. https://doi.org/10.1128/mBio.00209-20

40. TEJERO R, HUANG Y, RAMELOT T, MONTELIONE GT 2022 AlphaFold models of small proteins rival the accuracy of solution NMR structures. Front Mol Biosci 9: 877000. https://doi.org/10.3389/fmolb.2022.877000

41. HOOFT RW, SANDER C, VRIEND G 1997 Objectively judging the quality of a protein structure from a Ramachandran plot. Bioinformatics 13: 425-430. https://doi.org/10.1093/bioinformatics/13.4.425

42. KHO K 2021 A genomic approach to study cell wall biosynthesis in Staphylococcus aureus. PhD Thesis, Pennsylvania State University, USA

43. GOODARZI NN, BOLOURCHI N, FERESHTEH S, SHIRAZI AS, POURMAND MR, BADMASTI F 2021 Investigation of novel putative immunogenic targets against Staphylococcus aureus using a reverse vaccinology strategy. Infect Genet Evol 96: 105149. https://doi.org/10.1016/j.meegid.2021.105149

44. MANDAL MK, DOMB AJ 2024 Antimicrobial activities of natural bioactive polyphenols. Pharmaceutics 16(6): 718. https://doi.org/10.3390/pharmaceutics16060718

45. MASUMI M, NOORMOHAMMADI F, KIANISABA F, NOURI F, TAHERI M, TAHERKHANI A 2022 Methicillin-resistant Staphylococcus aureus: Docking-based virtual screening and molecular dynamics simulations to identify potential Penicillin-binding protein 2a inhibitors from natural flavonoids. Int J Microbiol 2022: 9130700. https://doi.org/10.1155/2022/9130700

46. GOGOI B, CHOWDHURY P, GOSWAMI N et al. 2021 Identification of potential plant-based inhibitor against viral proteases of SARS-CoV-2 through molecular docking, MM-PBSA binding energy calculations and molecular dynamics simulation. Mol Divers 25: 1963-1977. https://doi.org/10.1007/s11030-021-10211-9

47. VERMA AK, AHMED SKF, HOSSAIN MDS, et al. 2021 Molecular docking and simulation studies of flavonoid compounds against PBP-2a of methicillin-resistant Staphylococcus aureus. J Biomol Struct Dyn 40(21): 10561-10577. https://doi.org/10.1080/07391102.2021.1944911

48. VIJAYAKUMAR K, MUHILVANNAN S, ARUN VIGNESH M 2022 Hesperidin inhibits biofilm formation, virulence and staphyloxanthin synthesis in methicillin resistant Staphylococcus aureus by targeting SarA and CrtM: an in vitro and in silico approach. World J Microbiol Biotechnol 38(3): 44. https://doi.org/10.1007/s11274-022-03232-5

49. ESNAASHARI F, ZAHMATKESH H 2024 Antivirulence activities of rutin-loaded chitosan nanoparticles against pathogenic Staphylococcus aureus. BMC Microbiol 24: 328. https://doi.org/10.1186/s12866-024-03446-7

50. WANG S, XUE T, NIU B, WEI L, WANG H 2022 Preparation, characterization and antibacterial property of naringin loaded PLGA nanospheres. Prog Nat Sci Mater Int 32(4): 498-503. https://doi.org/10.1016/j.pnsc.2022.08.001